Chemical Science

EDGE ARTICLE

Table-salt enabled interface-confined synthesis of covalent organic framework (COF) nanosheets†

Xiansong Shi, Dongwei Ma, Fang Xu, Zhe Zhang and Yong Wang [ID] *

Two-dimensional covalent organic frameworks (COFs) are gaining tremendous interest for their potential applications in a diversity of fields. However, synthesis of COF nanosheets (CONs) usually suffers from tedious exfoliation processes and low yields. Herein, we present an exfoliation-free and scalable strategy to prepare few-layered CONs based on interface-confined synthesis, in which cheap and recyclable table salt (NaCl) is used as the sacrificial substrate. Salt particles are introduced into the reaction system, creating billions of solid–liquid interfaces. Oligomers formed upon the reaction between monomers are immediately adsorbed on salt surfaces, and the following polymerization leading to crystalline CONs is exclusively confined to salt surfaces. Salts can be easily removed by water washing, producing CONs with the thickness down to a few nanometers and lateral sizes up to hundreds of micrometers depending on the size of salt particles and the concentration of monomers. Four different kinds of CONs, both imine-linked and boron-containing, are synthesized from this generic method. As a demonstration, we prepare highly permeable and selective membranes using resultant CONs as building blocks. Thanks to the defect-free stacking of CONs with thin thicknesses and large lateral sizes on porous substrates, the membranes precisely separate similarly sized dyes while allowing ultrafast water permeation. This interface-confined strategy opens a new platform for the controllable and scalable synthesis of COF nanosheets and is essential for the burgeoning real-world applications of COFs in various fields.

Introduction

Covalent organic frameworks (COFs) have emerged as an attractive family of crystalline porous polymeric networks featured with predesigned geometries and functionalities.[1–5] Benefitting from their ordered inherent nanopores, atomically thin thickness, diverse topological structures, and facile functionalization, COFs have shown promising applications in a diversity of fields including gas adsorption,[6,7] catalysis,[8–10] ionic conduction and storage,[11,12] and membrane separation.[13–15] Typically, COFs are obtained in the form of insoluble and infusible micron-sized particulates through solvothermal synthesis.[16]

To take full advantage of the nanoporosity and two-dimensional (2D) structure of COFs, it is often required to use them in the form of thin COF nanosheets (CONs).[11,17,18] CONs with a few nanometers in thickness not only offer more active sites, but also improve mass transfer efficiency. These features significantly promote the performances of the devices assembled from CONs for applications such as sensing,[19,20] ion

conductivity,[11] and separation.[15,21] Unfortunately, turning these polymeric crystalline networks into thin nanosheets with a high yield remains a great challenge due to the strong π–π stacking interaction between adjacent COF monolayers. Extensive efforts have been devoted to synthesize CONs, and two main strategies, namely "top-down" and "bottom-up", have been developed for this purpose. The "top-down" strategy is usually conducted by exfoliating 2D layered COF particulates with the assistance of ultrasound,[22] solvent molecules,[23] or mechanical grinding.[24] However, this strategy is frequently limited by the entangled drawbacks of tedious exfoliation processes, low yields (<15%), and inhomogeneity in the size and thickness of the produced CONs. Importantly, Banerjee and coworkers developed new exfoliation methods, including chemically delamination by post modification[25] and self-exfoliation on guanidinium-based ionic COFs,[17] to produce high-quality CONs. Unfortunately, these approaches are only applicable to limited types of specially designed COFs. In contrast, the "bottom-up" synthesis is able to directly synthesize CONs with thicknesses down to the monolayer level. This strategy is usually realized with the assistance of interfaces which play an essential role in guiding the growth orientation of COFs. For instance, Wang and coworkers synthesized highly ordered COF monolayers on the surface of pyrolytic graphite by creating a solid–vapor interface.[26] Alternatively, by using solid–liquid interfaces, Dichtel *et al.* prepared

State Key Laboratory of Materials-Oriented Chemical Engineering, College of Chemical Engineering, Nanjing Tech University, Nanjing 211816, P. R. China. E-mail: yongwang@njtech.edu.cn

thin COF films on single-layer graphene and Au electrodes.[27,28] Bein *et al.* synthesized 2D COF films with tailored thicknesses on glass substrates *via* vapor-assisted conversion.[29] However, these "bottom-up" methods require the use of costly substrates and face the challenge of removing CONs from the substrates. Moreover, they are also suffering from issues including very low yields and poor scalability. Therefore, a cost-effective and scalable approach for the controllable synthesis of CONs is urgently needed and remains a great challenge.

There have been a large number of reports on the preparation of COF coatings on solid substrates with various materials and structures by solvothermal synthesis.[30–33] In these studies, COFs are formed both on the substrate surfaces as coating layers and in the bulk solutions as free particulates. Regrettably, in these uncontrolled syntheses of COFs, the majority of the COF monomers (typically >80%) are consumed by the reaction taking place in the bulk solution, resulting in undesired side products, free COF particulates. Even worse, the particulates may precipitate from the solution and contaminate the COF layers coated on the substrates. That is, under an "ideal" reaction condition where the reaction is exclusively confined to the substrate surfaces, all monomers will convert into COF nanosheets adhered to the substrate surfaces, leaving behind no particulates in the bulk solution. To this end, a strong interfacial confinement effect should be introduced in the reaction system. Interfaces are required here to guide the growth of COFs in one direction to generate 2D nanosheets or thin films. Moreover, the interfaces need to be present in the reaction with the confinement to suppress the growth of COFs in the bulk solution, thus avoiding the formation of free COF particulates. Hence, it is highly possible to convert all monomers into CONs if we can build sufficient confined interfaces during solvothermal synthesis. Herein, we report the scalable synthesis of various imine-linked and boron-based CONs through interface-confined solvothermal synthesis. By introducing a large number of salt particles in the reaction system, the growth of COFs is completely restricted on salt surfaces, producing well-defined CONs without the interference of any bulk particulates. Importantly, the CONs can be easily released from salts by water washing, implying their high efficiency and feasibility of mass production. The size and thickness of CONs can be regulated by changing salt sizes and monomer concentrations. Further, we use the thus-obtained imine-linked CONs as building blocks to prepare membranes by depositing them on porous substrates. The membranes exhibit remarkably high water permeances and tight selectivity, enabling fast separation of dyes with similar sizes.

Results and discussion

In this work, we prepared three kinds of imine-linked CONs, namely TpPa, TpBD, and TbPa, and the corresponding structures are shown in Fig. 1a. Fig. 1b illustrates the schematic diagram for the synthesis of CONs on small NaCl (sNaCl) particles with an average diameter of 12 μm. The obtained products are denoted as sNaCl@CONs. Here, the six facets of cubic NaCl crystals, which provide thermally stable surfaces that are nontoxic, cheap, and recyclable, serve as degradable substrates for the growth of CONs. Notably, the exclusive synthesis of CONs was realized by mixing monomers with a large number of NaCl particles (the mass of salts was 5000 times higher than that of the monomers). The salt particles were added into the monomer solution immediately after the mixing of the two monomers to create billions of confined solid–liquid (salt-solution) interfaces in the reaction system (Fig. S1†). The monomer solution was totally confined in the space among the tightly stacked salt particles, leading to the formation of the confined interface. Upon contact of the two monomers, condensation reactions take place, producing oligomers. Subsequently, the oligomers adsorb onto salt surfaces and grow into continuous and uniform CONs along the salt surfaces. The nanosheets can be readily released from salts by water washing. The successful synthesis of CONs was indicated
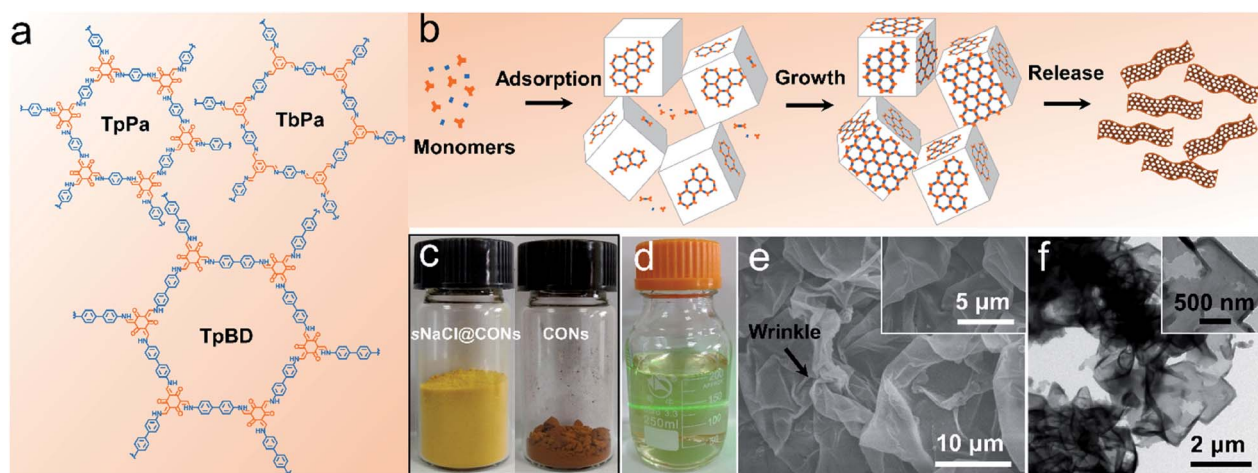

Fig. 1 Synthesis of imine-linked CONs by the interface-confined synthesis. (a) The molecular structure of TpPa, TpBD, and TbPa; (b) schematic of the preparation of TpPa CONs; (c) physical appearances of sNaCl@TpBD and released TpBD CONs; (d) dispersion of TpBD CONs in ethanol; (e and f) SEM and TEM images of TpPa CONs.

by the distinction in physical appearances of COF bulk particulates synthesized in the absence of salts, the products synthesized in the presence of salts (sNaCl@CONs), and released CONs by washing away salt particles (Fig. 1c, S2 and S3†). The strong Tyndall effect observed from the CON dispersion in ethanol clearly demonstrates the formation of thin nanosheets (Fig. 1d).[24] Scanning electron microscopy (SEM) and transmission electron microscopy (TEM) reveal that the released CONs possess wrinkled sheet-like structures with clear edges (Fig. 1e, f, and S4†), which are totally different from the petaled particulate morphology of COFs synthesized by the conventional solvothermal process without salts (Fig. S5†). As shown in Fig. 1f, the rectangular shape of the CON products implies the duplication of the cubic structure of the salt crystals during CON growth. The yields (mass$_{CONs}$/mass$_{monomers}$ × 100%) of the synthesis of CONs are 85.7%, 89.8%, and 88.3% for TpPa, TpBD and TbPa, respectively, which exhibit similar or higher conversion ratios of monomers compared with the synthesis of bulk COF particulates by the traditional solvothermal method (~85%).[34] The difference in the yields for three kinds of CONs might originate from the activity of precursors, the solubility of precursors in the solvent, and the oxygen content in the solvent. Importantly, we do not observe any free COF particulates in the obtained product (Fig. 1e and S4†), implying that COFs only grow along the surfaces of salt particles to form nanosheets.

The Fourier transform infrared (FTIR) spectra of the released CONs clearly indicate the formation of imine-linked frameworks. The TpPa and TpBD CONs show characteristic stretching bands at ~1575 cm^{-1} (–C=C) and ~1257 cm^{-1} (–C–N) (Fig. S6†). The disappearance of C=N stretching indicates that the tautomerization occurs in the synthesized CONs (Fig. S7†), implying that they hold a keto form.[35] The featured peak at ~1618 cm^{-1} for TbPa CONs also indicates the formation of imine bonds (Fig. S8†).[36] The disappearance of characteristic peaks originated from monomer pairs also implies the complete consumption of monomers after CON synthesis using this approach. Here, the peaks in FTIR spectra match well with the featured peaks of the corresponding COFs and do not show other redundant stretching bands, demonstrating that there is no side products left after removing salts by water washing. Powder X-ray diffraction (XRD) was then applied to ascertain the ordered structure of the COF particulates synthesized without salts and the released CONs. As shown in Fig. 2, column (i), both the COF particulates and CONs show clear peaks at lower 2θ values, for instance, TpPa (~4.7°), TpBD (~3.4°), and TbPa (~4.6°), which correspond to the reflections from the (100) plane. The XRD results clearly indicate that the thus-prepared CONs maintain their good crystallinity. Furthermore, the broad peak at a higher 2θ value about ~26–27° originates from the (001) plane reflection, indicating the π–π stacking between successive COF monolayers. Comparing the XRD results of particulates and CONs, a slight decrease in the intensity arising from the (100) plane reflection can be observed. This reduction could be caused by the random stacking of 2D COF sheets which contribute to the homogeneity of COF pores.[24] Besides, the (001) plane reflection of CONs is broadened or diminished
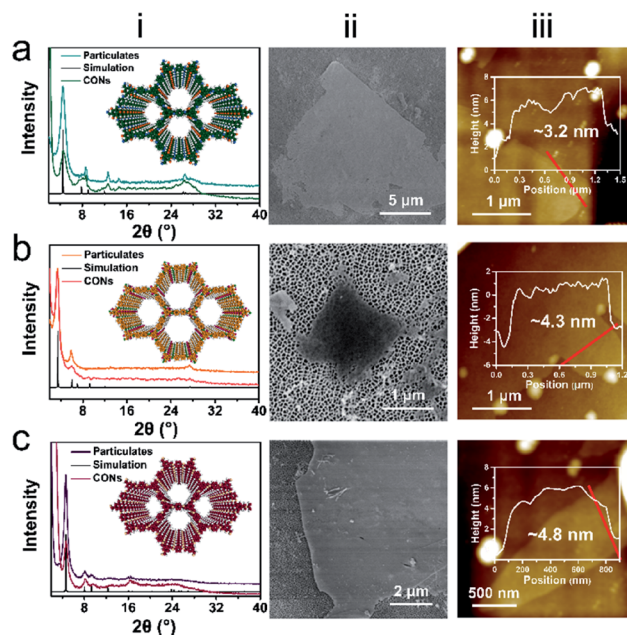

Fig. 2 Characterization of released CONs. (a) TpPa, (b) TpBD, (c) TbPa. XRD spectra (i), SEM images (ii), and AFM images (with the corresponding height profiles) (iii) are shown for the corresponding CONs.

compared with the COF particulates. The weakened peak here is believed to be due to the remarkable reduction in the number of the stacked layers in these CONs.[24] Importantly, compared with the XRD results of sNaCl@TpPa, we do not observe any peaks originated from the (200) plane of NaCl crystals (Fig. S9†), indicating that NaCl was completely removed after water washing. Given that the CONs are soaked in water for long duration to remove salts, the desired crystallinity exhibited by the resultant sheets demonstrates their excellent stability in water. Thermogravimetric analysis (TGA) was performed for TpPa CONs to obtain information about the thermal stability (Fig. S10†). The weight loss within 100 °C should be ascribed to the evaporation of water absorbed in the CON pores. The CONs show thermal stability up to 300 °C, and the gradual weight loss of nearly 100% is observed until 600 °C, corresponding to the complete decomposition of the nanosheets. Fig. 2, column (ii) shows the SEM images of CONs released from sNaCl crystals. These CONs show flat-sheet-like morphologies with lengths and widths of several micrometers. For instance, the average sheet sizes in width for TpPa, TpBD, and TbPa CONs deposited on anodic aluminum oxide (AAO) supports are 4.2, 1.0, and 2.9 μm, respectively (Fig. S11†). AFM characterization reveals that these imine-linked CONs present laminar structures with thicknesses ranging from ~3–5 nm (Fig. 2, column (iii)), corresponding to only ~10–15 COF monolayers (Fig. S12†).[37,38] Notably, TEM imaging clearly shows the staggered structure of the COF layers, which corresponds to the terrace structure observed from AFM images (Fig. S13†). Hence, we believe that, in the presence of a large amount of salt particles, CONs are formed by layer-by-layer growth between monomer pairs, thus producing layer-stacked frameworks. As shown above, this method is

applicable to the synthesis of different imine-linked CONs, and the synthesized few-layered sheets can be stably dispersed in ethanol (Fig. S14†). We then expanded this approach to synthesize other types of COFs to further demonstrate the universality of our method. For instance, the nanosheets of boron-based COF-1 were synthesized on sNaCl crystals. It can be clearly observed that COF-1 nanosheets with an average lateral size of about 0.5 μm are obtained after removing the salt crystals (Fig. S15†).

To reveal the formation mechanism of CONs on salts, we investigated the structural features of CONs grown on NaCl particles with different sizes. In addition to sNaCl particles with an average particle size of ~12 μm discussed above, big NaCl (bNaCl) particles with an average size of ~440 μm and a NaCl plate (2 cm × 2 cm × 0.3 cm) were also used as substrates to grow CONs by this approach (Fig. S16†). In the case of bNaCl particles, the prepared TpPa and TpBD CONs present lateral sizes of approximately 11 and 1.5 μm (Fig. S17 and S18†), respectively, which are much larger than those of CONs formed on sNaCl. Besides, the TpBD CON shows a thickness of about 12 nm (Fig. S19†), which is ~3 times higher than that of CONs synthesized on sNaCl particles. Also, the growth of COFs exclusively occurred on the surface of these bNaCl particles and no free COF particulates were formed in the bulk solution. Based on the above observations, we propose an interface-confined growth mechanism to elucidate the synthesis of CONs along the salt surfaces (Fig. 3a). Upon the contact between amine and aldehyde molecules, the coupling of reactive groups separately carried by two monomers leads to the formation of oligomers in the solution. Since NaCl particles possess a relatively high surface energy, the oligomers prefer to

adsorb onto salt surfaces and nucleation takes place, demonstrated by the color change of NaCl particles after a synthesis time of only 5 min (Fig. S20†). Also importantly, the salt-solution (solid–liquid) interface reduces the thermodynamic barrier and accelerates the kinetic control nucleation on the salt surface rather than homogeneous nucleation in the free solution.[39] The synergistic effect suppresses the growth of COFs in the free solution to form thermodynamically stable particulates, resulting in the complete condensation of monomers on the salt surface to generate sheet-like products. During the growth of CONs, the sufficient surface nucleation and adsorption of oligomers on salts lead to the merging of discrete nuclei with their neighbors to promote the lateral growth.

The subsequent reaction on the previously formed nuclei is responsible for the vertical growth in the thickness. Besides, the consumption of COF monomers limits the growth vertical to the salt surface, resulting in the formation of sheets with thin thicknesses. This nucleation-growth process of COF growth on solid–liquid interfaces can be confirmed by the distinction between the top and bottom morphologies, which are smooth and rough for the top and bottom, respectively (Fig. 3b). As the initial nucleation leads to an uneven growth of discrete nuclei, the CON side adhered to the salt surface features a rough texture. With further growth, the subsequently formed crystallites may repair this to produce a smooth surface. The lateral extension of sheets duplicates the texture of salt surfaces. To demonstrate this, we also prepared COFs on the NaCl plate with a rough surface (Fig. 3c). Obviously, a tortuous structure is obtained after removing the plate (Fig. 3d and S21†), implying the surface duplication during COF growth. Further, the extremely low dosage of monomer pairs compared to the salt particles leads to unsaturated growth of sheets, thus producing these sheets featuring a few nanometers in thickness (nanosheets). In the case of using bNaCl particles, as the used mass is the same as the sNaCl particles they provide greatly reduced surface areas for CON growth (Table S1†). Consequently, the unit area of the salt surface will share a higher monomer concentration, thus resulting in the formation of CONs with larger thicknesses. Notably, the nanosheets grown on both salt particles are not expected to cover the entire surface of the salt, leading to CONs with the lateral size much smaller than the particle size. By introducing a big 2 cm × 2 cm × 0.3 cm NaCl plate in the process, its surface is totally covered with continuous CONs (Fig. 3e) and a hollowed-out architecture built with these CONs is obtained after removing the plate (Fig. 3f). Notably, we find that there are many bulk COF particulates precipitated at the bottom of the autoclave after synthesis. These particulates are generated by the condensation of monomers in the free solution, implying the vital role of confined interfaces in synthesizing CONs on the substrate surfaces. The thickness of CONs formed on the salt plate is determined to be ~120 nm (Fig. S22†). That is, a thick COF film rather than thin nanosheets is generated on the surface of the salt plate. This complete coverage of the salt plate, which cannot be observed in the case of salt particles as the substrates, is also related to the accessible surface area for CON growth. The salt plate provides a surface area of ~10.4 cm² for CON growth, which is only
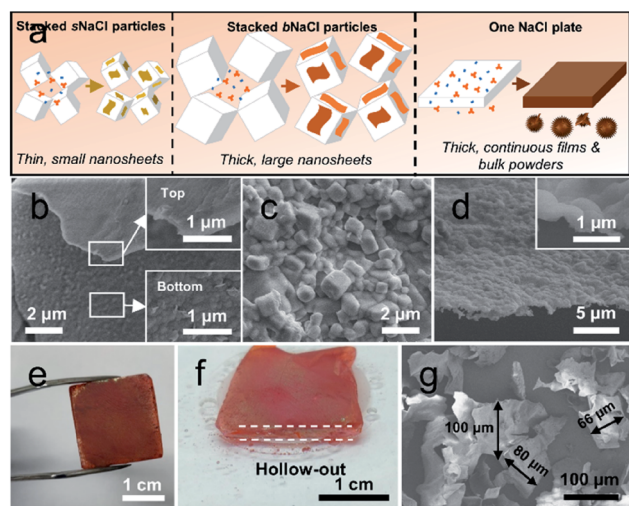

Fig. 3 Synthesis of CONs on salt substrates with different sizes. (a) Schematic presentation for the proposed mechanism; (b) top and bottom surfaces of CONs grown on bNaCl particles; (c) surface morphology of the rough salt plate; (d) cross-sectional morphology of the tortuous films released from the rough salt plate; (e) digital image of a salt plate with the COF film grown on its surface; (f) digital image of the COF film released from the salt plate; (g) released CONs synthesized with 30 times higher monomer concentration.

~0.02% of that of sNaCl particles (Table S1†). Interestingly, these continuous films can be transferred to other substrates to form composite structures (Fig. S23†). According to the proposed mechanism, increasing monomer concentration would also enhance the coverage of CONs on salt particles and produces CONs with larger lateral sizes. For example, when the monomer concentration was increased by 30 times, CONs with a greatly increased lateral size of approximately 100 μm are obtained (Fig. 3g). Following this method, high-quality CONs/films with well-controlled sizes and thicknesses can be obtained by tuning the monomer-to-area ratio. As only cheap, water-soluble, and recyclable salts are introduced into the solvothermal synthesis, our approach is much easier and more controllable compared to traditional methods including mechanical grinding and chemical exfoliation under harsh conditions (e.g., H_2SO_4/HNO_3, acetonitrile, and alkaline media).[40–42] More importantly, the mild synthesis strategy ensures the production of CONs with high crystallinity.

In the past decade, 2D materials possessing sheet-like structures in nanometer thicknesses, such as graphene oxide (GO) and derivatives,[43,44] delaminated metal–organic frameworks (MOFs),[45,46] and MXenes,[47,48] have attracted increasing interest in membrane separation. Different from nonporous 2D materials such as GO and MXenes, CONs possess permanent and highly ordered pores with diameters of about 1–3 nm. These pores provide additional channels for molecule permeation aside from the spaces between stacked layers if CONs are assembled to use as separation membranes (Scheme S3†).[49] This benefit will accordingly enhance the permeance of the CON-based membranes while maintaining tight selectivities. Considering that the facile production of CONs with the assistance of salt substrates is realized in the present work without any tedious delamination, we sought to use these CONs as building blocks to fabricate membranes for molecular separations. TpPa and TpBD CONs, which are highly water stable in nature,[35] had the lateral size of a few micrometers after being released from sNaCl and were used as building blocks to produce membranes. A home-made vacuum filtration device (Fig. 4a and S24†) was used to assemble these 2D CONs onto porous AAO substrates. The thus-deposited CON layer possessed a stacked structure of nanosheets (Fig. 4b). As shown in Fig. 4c, the physical appearance change after CON deposition, indicating the successful deposition of CON layers, and the prepared membranes are almost optically transparent, implying the thin thickness of the deposited CON layer. Distinctly different from the AAO substrates having ~20 nm pores (Fig. 4d), the TpPa and TpBD CONs achieve a complete and relatively smooth coverage on the substrate without any visible defects (Fig. 4e and f). We can observe some sharp edges in the SEM image (boxed area in Fig. 4e, f, and S25†) because of the sheet-like structure of CONs. The cross-sectional morphology of the membrane displays a thin CON layer tightly adhered to the AAO substrate and the thickness of the CON layer is about 250 nm (Fig. 4g). The produced membranes still maintain a moderate hydrophilicity facilitating water permeation (Fig. S26†).

The prepared CON-AAO composite membranes were used to separate a series of dye molecules in water to demonstrate their potential application in molecular separation. Dispersions of TpBD CONs were first measured by UV-vis spectroscopy and a linear relationship between absorbance and CONs concentration can be observed (Fig. S27†). Thus, the thickness of the membranes built using CONs corresponds to the filtered amount of the CON dispersion, suggesting that a controllable separation performance can be realized. Here, the amount of the used CONs for membrane fabrication was presented by using the dosage of sNaCl@CONs. The separation performance of the produced membranes was first evaluated by filtration of
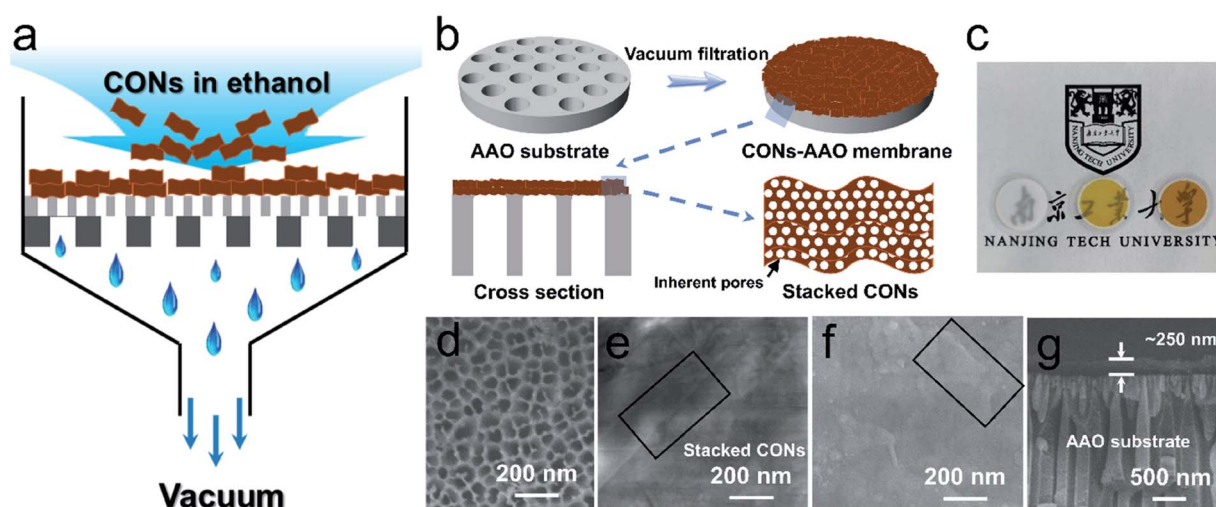

Fig. 4 Deposition of imine-linked CONs on AAO supports to prepare composite membranes with CONs as the selective layer. (a) Schematic presentation for membrane fabrication by vacuum filtration; (b) schematic presentation shows the surface and cross-sectional structure of the composite membrane; (c) photographs of AAO supports (left), TpBD-AAO (middle), and TpPa-AAO (right) composite membranes, respectively, and the corresponding surface morphologies (d–f); (g) cross-sectional morphology of the TpPa-AAO composite membrane. Boxed areas in (e and f) show the stacked CON morphology.

Evans blue (EB). Fig. 5a shows the relationship between the dosage of sNaCl@TpPa and permselectivity. Notably, the 20 nm AAO substrate possesses a water permeance of $\sim$2148 L m^{-2} h^{-1} bar^{-1} but negligible rejection of EB (<10%). After depositing CONs released from only 40 mg sNaCl@TpPa (denoted as TpPa$_{40}$-AAO), the rejection of EB is improved to $\sim$48.2% and water permeance is decreased to $\sim$897 L m^{-2} h^{-1} bar^{-1}. Increasing the sNaCl@TpPa dosage from 50 mg to 70 mg significantly elevates the rejection from $\sim$62.1% to $\sim$93.5% accompanied by reduced permeance from $\sim$581 to $\sim$191 L m^{-2} h^{-1} bar^{-1}.

With 80 mg of dosage, we achieve a rejection of $\sim$99.2% and a water permeance still as high as $\sim$122 L m^{-2} h^{-1} bar^{-1}. Similarly, for the composite membranes with the deposited TpBD CONs as the selective layers, the water permeance and rejection rate display an opposite tendency with increasing dosages of sNaCl@TpBD (Fig. 5b). Eventually, the TpBD$_{80}$-AAO membrane presents a rejection of $\sim$99.2% and a decent water permeance of $\sim$89 L m^{-2} h^{-1} bar^{-1}. Importantly, the water permeance of the thus-produced membranes displays an approximately linear reduction with the increase of the CON dosage, matching well with the Hagen–Poiseuille equation.[50] Here, the membrane thickness is gradually increased with increasing dosage of CONs, thus producing more and longer transporting routes to effectively sieve dye molecules.[51] For this reason, the rejection of solutes presents a gradually improved tendency while the water permeance declines because of the increased mass transfer resistance. To further assess the separation performance of the CON-based membranes, a series of low molecular weight dyes with molecular weight (M_w) ranging

from $\sim$300 to 1000 Da were used in the rejection tests. As shown in Fig. 5c, the rejection rates for various dyes are gradually improved with increasing M_w, demonstrated by the visible change in color during filtration (inset in Fig. 5c) and UV-vis spectra (Fig. S28†). Moreover, the molecular weight cut-off (MWCO) of TpBD$_{80}$-AAO is determined to be $\sim$780 Da based on the 90% rejection of molecules. The TpBD$_{80}$-AAO membrane was then subjected to a mixture containing methyl orange (MO) and EB to verify the molecular sieving effect. As illustrated in Fig. 5d, the membrane selectively allows the passage of MO molecules (yellow) from the green feed [resulting from blue (EB) and yellow (MO)] (Fig. S29†), which is further confirmed by the UV-vis spectra (Fig. 5e). In addition, the prepared membranes show very stable performance in rejection after a long-term test over a period of 30 h benefiting from the stability of CONs (Fig. 5f and S30†). The moderate reduction ($\sim$25%) in water permeance should be caused by the concentration polarization during the continuous dyed water filtration.[52] Remarkably, the synergistic effect of ordered nanopores and few-layered CONs endows the membranes with excellent rejection rates and remarkably high water permeances, which are $\sim$2–10 times higher than those of membranes built by other 2D materials, e.g. MOFs and GO as building blocks (Fig. 5g and Table S2†). Compared with the TpPa-AAO membrane whose selective layer is built by directly growing TpPa crystallites on the porous substrate,[53] a nearly 10-fold improvement in water permeance with similar rejections also convincingly demonstrates the advantage of the COF-based membranes assembled by thin nanosheets. Hence, the membranes prepared with the synthesized CONs present an excellent and stable performance,
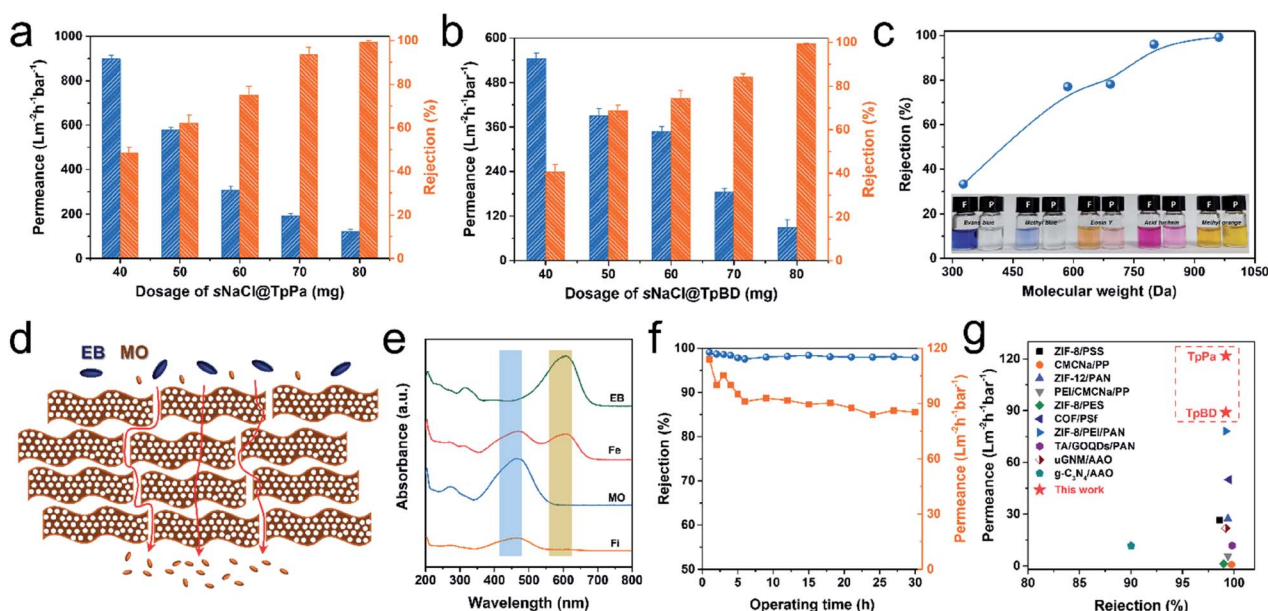

Fig. 5 Separation performances of CON-AAO composite membranes. (a and b) Performance of TpPa and TpD membranes prepared from different sNaCl@CON dosages; (c) the rejection of dyes with different molecular weights of TpBD membranes; (d) schematic presentation for the molecular sieving mechanism through the stacked TpBD CON layer; (e) UV-vis spectra corresponding to the selective removal of EB from a MO and EB mixture; (f) rejection and dyed water permeance in a long-time separation of EB; (g) comparison of separation performance of our membranes with other membranes (for details see Table S1†).

indicating their great potential in molecular separations. CONs synthesized on small salt particles from the confined-interface strategy exhibit thin thicknesses and large lateral sizes. Because of this large surface area/thickness ratio, these CONs can fully cover the surface of the porous substrates at a low deposition thickness by vacuum filtration, thus forming a thin yet defect-free selective layer. Consequently, small molecules like water quickly pass through the intrinsic ~2 nm pores in the CON layers while big molecules are rejected, showing an excellent molecular separation performance.

Conclusions

In summary, we present a facile and controllable interface-confined strategy for the scalable synthesis of COF nanosheets, which is generally applicable to various types of COFs. Stacked NaCl crystals, as cheap, water-soluble, and recyclable templates, guide the direct and exclusive growth of CONs on their surfaces without the interference of bulk particulates in the free solution. The as-synthesized imine-linked CONs/films show broadly tunable lateral dimensions from ~1 μm to ~2 cm with thicknesses ranging from ~3 nm to ~120 nm determined by salt sizes and growth conditions. The vacuum filtration enables the assembly of defect-free CON layers on porous substrates, producing composite membranes with assembled CONs as the selective layers with highly controllable thicknesses. The thus-prepared membranes exhibit tight rejections of dyes and remarkable permeance much higher than other membranes with similar rejections prepared by other methods. Because of the distinguished features in terms of controllability, scalability, and generality, this interface-confined strategy for the synthesis of CONs is expected to play an important role in boosting the real-world applications of CONs in a large variety of fields.

Conflicts of interest

There are no conflicts to declare.

Acknowledgements

Notes and references

1 A. P. Cote, A. I. Benin, N. W. Ockwig, M. O'Keeffe, A. J. Matzger and O. M. Yaghi, *Science*, 2005, **310**, 1166–1170.

2 C. Zhao, C. S. Diercks, C. Zhu, N. Hanikel, X. Pei and O. M. Yaghi, *J. Am. Chem. Soc.*, 2018, **140**, 16438–16441.

3 L. H. Li, X. L. Feng, X. H. Cui, Y. X. Ma, S. Y. Ding and W. Wang, *J. Am. Chem. Soc.*, 2017, **139**, 6042–6045.

4 S. Y. Ding and W. Wang, *Chem. Soc. Rev.*, 2013, **42**, 548–568.

5 M. S. Lohse and T. Bein, *Adv. Funct. Mater.*, 2018, **28**, 1705553.

6 C. J. Doonan, D. J. Tranchemontagne, T. G. Glover, J. R. Hunt and O. M. Yaghi, *Nat. Chem.*, 2010, **2**, 235–238.

7 A. F. M. El-Mahdy, C.-H. Kuo, A. Alshehri, C. Young, Y. Yamauchi, J. Kim and S.-W. Kuo, *J. Mater. Chem. A*, 2018, **6**, 19532–19541.

8 S.-Y. Ding, J. Gao, Q. Wang, Y. Zhang, W.-G. Song, C.-Y. Su and W. Wang, *J. Am. Chem. Soc.*, 2011, **133**, 19816–19822.

9 R. Chen, J. L. Shi, Y. Ma, G. Lin, X. Lang and C. Wang, *Angew. Chem., Int. Ed.*, 2019, **58**, 6430–6434.

10 P. Pachfule, A. Acharjya, J. Roeser, T. Langenhahn, M. Schwarze, R. Schomacker, A. Thomas and J. Schmidt, *J. Am. Chem. Soc.*, 2018, **140**, 1423–1427.

11 H. Chen, H. Tu, C. Hu, Y. Liu, D. Dong, Y. Sun, Y. Dai, S. Wang, H. Qian, Z. Lin and L. Chen, *J. Am. Chem. Soc.*, 2018, **140**, 896–899.

12 M. S. Kim, W. J. Lee, S. M. Paek and J. K. Park, *ACS Appl. Mater. Interfaces*, 2018, **10**, 32102–32111.

13 K. Dey, M. Pal, K. C. Rout, H. S. Kunjattu, A. Das, R. Mukherjee, U. K. Kharul and R. Banerjee, *J. Am. Chem. Soc.*, 2017, **139**, 13083–13091.

14 W. Zhang, L. Zhang, H. Zhao, B. Li and H. Ma, *J. Mater. Chem. A*, 2018, **6**, 13331–13339.

15 D. B. Shinde, G. Sheng, X. Li, M. Ostwal, A. H. Emwas, K. W. Huang and Z. Lai, *J. Am. Chem. Soc.*, 2018, **140**, 14342–14349.

16 S. Kandambeth, V. Venkatesh, D. B. Shinde, S. Kumari, A. Halder, S. Verma and R. Banerjee, *Nat. Commun.*, 2015, **6**, 6786.

17 S. Mitra, S. Kandambeth, B. P. Biswal, M. A. Khayum, C. K. Choudhury, M. Mehta, G. Kaur, S. Banerjee, A. Prabhune, S. Verma, S. Roy, U. K. Kharul and R. Banerjee, *J. Am. Chem. Soc.*, 2016, **138**, 2823–2828.

18 A. Mal, R. K. Mishra, V. K. Praveen, M. A. Khayum, R. Banerjee and A. Ajayaghosh, *Angew. Chem., Int. Ed.*, 2018, **57**, 8443–8447.

19 G. Das, B. P. Biswal, S. Kandambeth, V. Venkatesh, G. Kaur, M. Addicoat, T. Heine, S. Verma and R. Banerjee, *Chem. Sci.*, 2015, **6**, 3931–3939.

20 C. Zhang, S. Zhang, Y. Yan, F. Xia, A. Huang and Y. Xian, *ACS Appl. Mater. Interfaces*, 2017, **9**, 13415–13421.

21 G. Li, K. Zhang and T. Tsuru, *ACS Appl. Mater. Interfaces*, 2017, **9**, 8433–8436.

22 I. Berlanga, M. L. Ruiz-Gonzalez, J. M. Gonzalez-Calbet, J. L. Fierro, R. Mas-Balleste and F. Zamora, *Small*, 2011, **7**, 1207–1211.

23 D. N. Bunck and W. R. Dichtel, *J. Am. Chem. Soc.*, 2013, **135**, 14952–14955.

24 S. Chandra, S. Kandambeth, B. P. Biswal, B. Lukose, S. M. Kunjir, M. Chaudhary, R. Babarao, T. Heine and R. Banerjee, *J. Am. Chem. Soc.*, 2013, **135**, 17853–17861.

25 M. A. Khayum, S. Kandambeth, S. Mitra, S. B. Nair, A. Das, S. S. Nagane, R. Mukherjee and R. Banerjee, *Angew. Chem., Int. Ed.*, 2016, **55**, 15604–15608.

26 X. H. Liu, C. Z. Guan, S. Y. Ding, W. Wang, H. J. Yan, D. Wang and L. J. Wan, *J. Am. Chem. Soc.*, 2013, **135**, 10470–10474.

27 J. W. Colson, A. R. Woll, A. Mukherjee, M. P. Levendorf, E. L. Spitler, V. B. Shields, M. G. Spencer, J. Park and W. R. Dichtel, *Science*, 2011, **332**, 228–231.

28 C. R. DeBlase, K. Hernandez-Burgos, K. E. Silberstein, G. G. Rodriguez-Calero, R. P. Bisbey, H. D. Abruna and W. R. Dichtel, *ACS Nano*, 2015, **9**, 3178–3183.

29 D. D. Medina, J. M. Rotter, Y. Hu, M. Dogru, V. Werner, F. Auras, J. T. Markiewicz, P. Knochel and T. Bein, *J. Am. Chem. Soc.*, 2015, **137**, 1016–1019.

30 H. W. Fan, J. H. Gu, H. Meng, A. Knebel and J. Caro, *Angew. Chem., Int. Ed.*, 2018, **57**, 4083–4087.

31 H. Lu, C. Wang, J. J. Chen, R. Ge, W. G. Leng, B. Dong, J. Huang and Y. A. Gao, *Chem. Commun.*, 2015, **51**, 15562–15565.

32 H. Fan, A. Mundstock, A. Feldhoff, A. Knebel, J. Gu, H. Meng and J. Caro, *J. Am. Chem. Soc.*, 2018, **140**, 10094–10098.

33 T. Sick, A. G. Hufnagel, J. Kampmann, I. Kondofersky, M. Calik, J. M. Rotter, A. Evans, M. Doblinger, S. Herbert, K. Peters, D. Bohm, P. Knochel, D. D. Medina, D. Fattakhova-Rohlfing and T. Bein, *J. Am. Chem. Soc.*, 2018, **140**, 2085–2092.

34 Z. Kang, Y. Peng, Y. Qian, D. Yuan, M. A. Addicoat, T. Heine, Z. Hu, L. Tee, Z. Guo and D. Zhao, *Chem. Mater.*, 2016, **28**, 1277–1285.

35 S. Kandambeth, A. Mallick, B. Lukose, M. V. Mane, T. Heine and R. Banerjee, *J. Am. Chem. Soc.*, 2012, **134**, 19524–19527.

36 Y. Peng, W. K. Wong, Z. Hu, Y. Cheng, D. Yuan, S. A. Khan and D. Zhao, *Chem. Mater.*, 2016, **28**, 5095–5101.

37 T.-Y. Zhou, F. Lin, Z.-T. Li and X. Zhao, *Macromolecules*, 2013, **46**, 7745–7752.

38 K. Baek, G. Yun, Y. Kim, D. Kim, R. Hota, I. Hwang, D. Xu, Y. H. Ko, G. H. Gu, J. H. Suh, C. G. Park, B. J. Sung and K. Kim, *J. Am. Chem. Soc.*, 2013, **135**, 6523–6528.

39 H. Wang, B. He, F. Liu, C. Stevens, M. A. Brady, S. Cai, C. Wang, T. P. Russell, T. W. Tan and Y. Liu, *J. Mater. Chem. C*, 2017, **5**, 5090–5095.

40 Y. Zhu, X. Chen, Y. Cao, W. Peng, Y. Li, G. Zhang, F. Zhang and X. Fan, *Chem. Commun.*, 2019, **55**, 1434–1437.

41 X. Lan, C. Du, L. Cao, T. She, Y. Li and G. Bai, *ACS Appl. Mater. Interfaces*, 2018, **10**, 38953–38962.

42 P. Peng, L. Shi, F. Huo, S. Zhang, C. Mi, Y. Cheng and Z. Xiang, *ACS Nano*, 2019, **13**, 878–884.

43 A. Akbari, P. Sheath, S. T. Martin, D. B. Shinde, M. Shaibani, P. C. Banerjee, R. Tkacz, D. Bhattacharyya and M. Majumder, *Nat. Commun.*, 2016, **7**, 10891.

44 K. H. Thebo, X. Qian, Q. Zhang, L. Chen, H. M. Cheng and W. Ren, *Nat. Commun.*, 2018, **9**, 1486.

45 Y. Peng, Y. Li, Y. Ban and W. Yang, *Angew. Chem., Int. Ed.*, 2017, **56**, 9757–9761.

46 H. Ang and L. Hong, *ACS Appl. Mater. Interfaces*, 2017, **9**, 28079–28088.

47 L. Ding, Y. Wei, L. Li, T. Zhang, H. Wang, J. Xue, L.-X. Ding, S. Wang, J. Caro and Y. Gogotsi, *Nat. Commun.*, 2018, **9**, 155.

48 L. Ding, Y. Wei, Y. Wang, H. Chen, J. Caro and H. Wang, *Angew. Chem., Int. Ed.*, 2017, **56**, 1825–1829.

49 V. Kuehl, J. Yin, P. Duong, B. Mastorovich, B. S. Newell, K. D. Li-Oakey, B. A. Parkinson and J. O. Hoberg, *J. Am. Chem. Soc.*, 2018, **140**, 18200–18207.

50 J. Cai, E. Perfect, C.-L. Cheng and X. Hu, *Langmuir*, 2014, **30**, 5142–5151.

51 C. Chen, J. Wang, D. Liu, C. Yang, Y. Liu, R. S. Ruoff and W. Lei, *Nat. Commun.*, 2018, **9**, 1902.

52 N. Endre, K. Edina and N. Andras, *J. Membr. Sci.*, 2011, **368**, 215–222.

53 X. Shi, A. Xiao, C. Zhang and Y. Wang, *J. Membr. Sci.*, 2019, **576**, 116–122.